

## Controllable continuous variable quantum state distributor: supplement

QINGWEI WANG,<sup>1,†</sup> YAJUN WANG,<sup>1,2,†</sup>  XIAOCONG SUN,<sup>1</sup> YUHANG TIAN,<sup>1</sup> WEI LI,<sup>3</sup> LONG TIAN,<sup>1,2</sup> XUDONG YU,<sup>1,2</sup> JING ZHANG,<sup>1,2,4</sup> AND YAOHUI ZHENG<sup>1,2,\*</sup> 

<sup>1</sup>State Key Laboratory of Quantum Optics and Quantum Optics Devices, Institute of Opto-Electronics, Shanxi University, Taiyuan 030006, China

<sup>2</sup>Collaborative Innovation Center of Extreme Optics, Shanxi University, Taiyuan, Shanxi 030006, China

<sup>3</sup>College of Physics and Electronic Engineering, Shanxi University, Taiyuan, Shanxi, 030006, China

<sup>4</sup>e-mail: jzhang74@yahoo.com

\*Corresponding author: yzheng@sxu.edu.cn

<sup>†</sup>These authors contributed equally to this Letter.

---

This supplement published with The Optical Society on 6 April 2021 by The Authors under the terms of the [Creative Commons Attribution 4.0 License](https://creativecommons.org/licenses/by/4.0/) in the format provided by the authors and unedited. Further distribution of this work must maintain attribution to the author(s) and the published article's title, journal citation, and DOI.

Supplement DOI: <https://doi.org/10.6084/m9.figshare.14153318>

Parent Article DOI: <https://doi.org/10.1364/OL.419261>

# Supplementary Document for “Controllable continuous variables quantum state distributor”

Additional information about the Controllable continuous variable quantum state distributor is as follows: Sec. I, Generation of entangled Einstein-Podolsky-Rosen (EPR) beam. Sec. II, Investigation of Continuous variable 1→2 quantum state distributor. Sec. III, Investigation of 1→M quantum state distributor. Sec. IV, Fidelity of multistep quantum state distributor. Sec. V, Information of the quantum state in the semi-quantum channel.

## Generation of the entangled EPR beam.

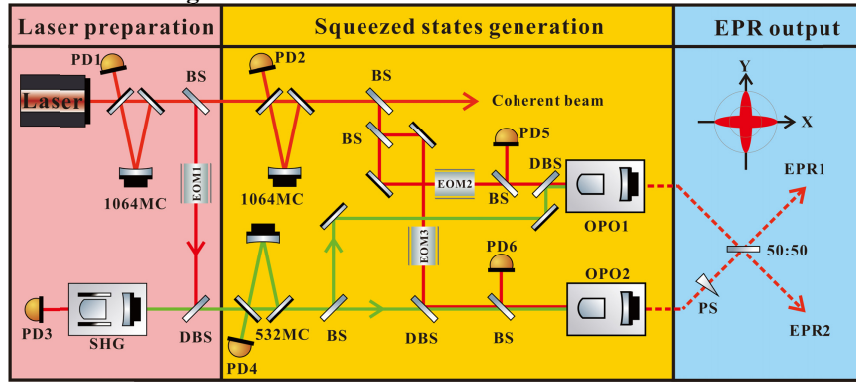


Fig. S1. Schematic of the entangled EPR beam generation. MC, mode cleaner; PD, photodetector; BS, beam splitter; DBS, dichroic beam splitter; EOM, electro-optical modulator; SHG, second harmonic generation; OPO, optical parametric oscillator; PS, phase shifter.

The schematic for the generation of the entangled EPR beams is illustrated in Fig. S1. The laser source of our experiment is a home-made Nd:YVO4 ring laser with 2.5 W continuous-wave single-frequency output power at 1064 nm. The laser transmits through a mode cleaner which provides spatial-temporal filtering, polarization purifying for the downstream experiment. Most of the laser power is used for the second-harmonic generation to provide the pump field at 532 nm for our OPOs. The other two mode cleaners are positioned in the beam paths of both the local oscillator and pump field to serve as an optical filter for phase noise. Both two optical parameter amplifiers (OPOs) are semi-monolithic single-resonant standing wave cavity, consisting of a piezo-actuated concave mirror and a periodically poled KTiOPO4 (PPKTP) crystal with a dimension of 1mm×2mm×10mm. The crystal end face with a radius of curvature of 12 mm is coated as high reflectivity for the fundamental field and high transmission for the pump field, thus serving as the cavity end mirror. The plane front face of the crystal is coated as antireflectivity for both wavelengths. An air gap of 27 mm length is realized between the antireflectivity-coated side of the crystal and the coupling mirror. The concave mirror with a radius of curvature of 30 mm has a transmissivity of 12%±1.5% for 1064 nm and HR for 532 nm, which is used as the output coupler. Three home-made electro-optic modulations (EOMs) with the modulation frequency of 56.4 MHz (EOM1), 35.6 MHz (EOM2), and 34.8 MHz (EOM3) are applied to actively lock the length of the resonators and relative phases [1]. The relative phases between the seed and pump beams of the OPOs are locked to  $\pi$ . Detailed information for the generation of the squeezed states is illustrated in ref [2, 3]. After the production of the two single mode states, they are directed toward a balanced beam splitter to produce the EPR entangled beams with a relative phase of  $\pi/2$ .

Here, we suppose that there are two single mode squeezed states with the same squeezing factors  $r$ , which can be expressed as

$$\hat{S}_1 = \hat{a}_1 \cosh r - \hat{a}_1^\dagger \sinh r \quad (\text{S1})$$

$$\hat{S}_2 = \hat{a}_2 \cosh r - \hat{a}_2^\dagger \sinh r \quad (\text{S2})$$

where  $\hat{a}_1$  and  $\hat{a}_2$  are the annihilation operators of the two squeezed states. The two squeezed states are coupled on a 50:50 beam splitter with the relative phase of  $\pi/2$ . The output beams are entangled, which can be expressed as

$$\hat{E}_1 = \frac{\sqrt{2}}{2}(\hat{S}_1 + i\hat{S}_2) = \frac{\sqrt{2}}{2}(\hat{a}_1 \cosh r - \hat{a}_1^\dagger \sinh r + i\hat{a}_2 \cosh r - i\hat{a}_2^\dagger \sinh r) \quad (\text{S3})$$

$$\hat{E}_2 = \frac{\sqrt{2}}{2}(\hat{S}_1 - i\hat{S}_2) = \frac{\sqrt{2}}{2}(\hat{a}_1 \cosh r - \hat{a}_1^\dagger \sinh r - i\hat{a}_2 \cosh r + i\hat{a}_2^\dagger \sinh r) \quad (\text{S4})$$

The squeezing factor  $r$  is measured under different OPO1 pump factors (ratio of the pump power to the threshold power). The threshold power of the OPO1 is about 163 mW, while the OPO2 has a threshold power of 193 mW. The dependence of the squeezing factor  $r$  on the pump factor is no obvious difference with that of the OPO1, which is omitted. Ideally, the squeezing factor of the generated entanglement state has the same value as the squeezing factor of the originally squeezed states. The squeezing factor of the entanglement state reaches the maximum value at the threshold power of 80%. The maximum squeezing degree is measured to be 13.8 dB below the shot noise limit, close to the record of 15 dB [4]. Here, in order to reduce the influence of anticorrelation noise on the fidelity, both two OPOs operate at the threshold power of 60%. Due to the additional propagation loss of the EPR beams, the ultimate squeezing factor of the entanglement state is less than that of the original squeezed state, corresponding to a maximum squeezing factor of 1.128. Thus, in the experiment, we can manipulate the squeezing factor from 0 to 1.128 by changing the pump power of the OPO.

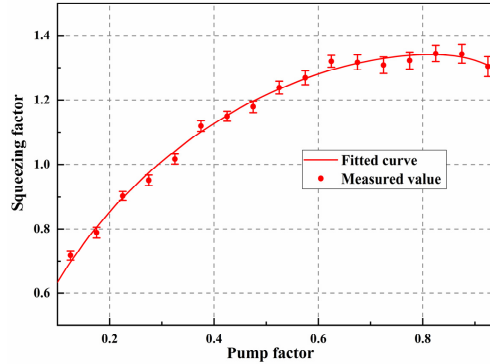


Fig. S2. Dependence of the squeezing factor on the pump factor (ratio of the pump power to the threshold power). The separated dot is the measured result in the experiment, the solid line is the fitted curve.

### Investigation of Continuous variable 1→2 quantum state distributor

The schematic diagram of the continuous variable (CV) quantum state distributor is shown in Fig. S3. Similar to quantum teleportation operation [5], a CV EPR entanglement beam is employed to manipulate the distribution of the quantum state. The EPR beam is distributed to the Sender and Distributor to help the storage and reconstruction of the quantum

state. Partial information of the original quantum state from node 1  $\hat{a}_{in}$  is extracted with the help of one half of the EPR beam and then stored in a displaced state  $\hat{a}_{disp}$ . The displaced state is then transmitted to the Distributor through the semi-quantum channel and the initial quantum state is reconstructed with the assistance of the other half of the EPR beam. The fidelity at two output nodes, as an indicator of quantifying the distribution process, is dependent of the correlation noise  $V(r, \theta)$  of the EPR beam. The fidelity of only one node may be superior to the classical limit, with no violation of the no-cloning theorem. The fidelities of the two nodes have the opposite trend as the squeezing factor  $r$  is increased. In addition, the fidelities can be switched between the two nodes with the squeezing angle  $\theta$ . Therefore, the schematic diagram exactly achieves the controllable quantum state distributor and the Wigner function of the distributed state could be obtained at the receivers' nodes [6]. The data acquired by SA is shown in the main text in Fig.3 and the data acquired by the OSC is shown as the reconstructed Wigner function in Fig. S3.

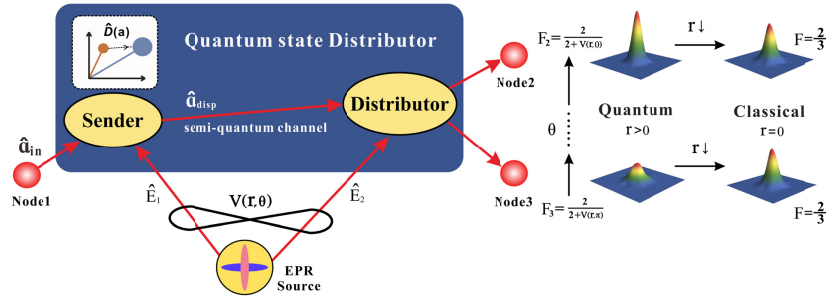


Fig. S3. Schematic diagram of the continuous variable quantum state distributor. EPR source has two sub-modes  $\hat{E}_1$  and  $\hat{E}_2$ . The initial state  $\hat{a}_{in}$  is converted into the displaced state  $\hat{a}_{disp}$  with the aid of the sub-mode  $\hat{E}_1$ . Subsequently, the output state is retrieved using the displaced state  $\hat{a}_{disp}$  and sub-mode  $\hat{E}_2$ . The fidelities of  $\hat{a}_{out2}$  and  $\hat{a}_{out3}$  are dependent of the correlation variance.

In the proposal, an unknown state from node 1 is described using the electromagnetic field annihilation operator  $\hat{a}_{in}$ , which can be expressed in terms of the amplitude  $\hat{X} = \hat{a} + \hat{a}^\dagger$  and phase  $\hat{Y} = -i(\hat{a} - \hat{a}^\dagger)$  quadratures with a canonical commutation relation  $[\hat{X}, \hat{Y}] = 2i$ .  $\hat{a}$  and  $\hat{a}^\dagger$  are the photon annihilation and creation operators for a single-mode field, respectively.

After the signal field entering the Sender, it first passes through a beam splitter with a reflectivity of  $R$ . The transmitted and reflected fields are  $\hat{c} = \sqrt{1-R}\hat{a}_{in} - \sqrt{R}\hat{V}_1$  and  $\hat{d} = \sqrt{1-R}\hat{a}_{in} + \sqrt{R}\hat{V}_1$ , respectively. The vacuum noise  $\hat{V}_1$  is introduced by the other side of the beam splitter.

Secondly, the reflected field meets EPR1 at a balanced beam splitter and the information of the two output ports of the beam splitter are extracted and stored by two balanced homodyne detectors with the help of two local oscillators.

Thirdly, the stored information modulates the amplitude and phase quadrature of an auxiliary beam by two independent modulators with the same gain factor of  $g$ . The auxiliary beam then displaces the transmission signal field at a beam splitter of 1:99 (with the relative phase of 0) as

$$\hat{a}_{disp} = (\sqrt{1-R} + \frac{g\sqrt{R}}{\sqrt{2}})\hat{a}_{in} + (\sqrt{R} - \frac{g\sqrt{1-R}}{\sqrt{2}})\hat{V}_1 - \frac{g}{\sqrt{2}}\hat{E}_1^+ \quad (S5)$$

when  $g$  is set to  $\sqrt{2R/(1-R)}$ , the vacuum noise is vanished, the displaced field is given by

$$\hat{a}_{disp}^c = \frac{1}{\sqrt{1-R}} \hat{a}_{in} - \sqrt{\frac{R}{1-R}} \hat{E}_1^+ \quad (S6)$$

In order to optimize the gain of the classical channel, sinusoidal signals with the amplitude of 20 dB are imposed on the amplitude and phase modulators as the input state, respectively. The gain of the electronic signal is carefully calibrated by an adjustable attenuator, the calibration is completed when the observed signal of the transmitted quantum state at Victor's station is 20 dB above the shot noise limit.

After another beam splitter with the same reflectivity of  $R$ , the output states from two output parts of beam splitter are written by

$$\hat{a}_{out2} = \hat{a}_{in} - \sqrt{R}(\hat{E}_1^+ + \hat{E}_2 e^{i\theta}) \quad (S7)$$

$$\hat{a}_{out3} = \sqrt{\frac{R}{1-R}} \hat{a}_{in} - \frac{R}{\sqrt{1-R}} \hat{E}_1^+ + \sqrt{1-R} \hat{E}_2 e^{i\theta} \quad (S8)$$

where  $\theta$  is the relative phase between the displaced field and EPR2. They correspond to the output states for the two paths of the distributor, which will be sent to two different nodes.

The fidelity is defined as  $F \equiv \langle \psi^{in} | \hat{\rho}^{out} | \psi^{in} \rangle$  in which ‘‘in’’ and ‘‘out’’ denote the input and output state [7]. In the case of unity gain, the fidelity for Gaussian state can be simply given by

$$F = \frac{2}{\sqrt{(1 + \langle \delta \hat{X}_{out}^2 \rangle)(1 + \langle \delta \hat{Y}_{out}^2 \rangle)}} \quad (S9)$$

where  $\delta \hat{X}_{out}^2$ ,  $\delta \hat{Y}_{out}^2$  are the variances of the quadrature amplitude and phase components, respectively.

In the case of  $R=1/2$ , only half the information of the unknown quantum state is destroyed. For the classical case of  $r=0$ , the fidelity of both  $\hat{a}_{out2}$  and  $\hat{a}_{out3}$  are  $2/3$ , this scheme corresponds to the optimal fidelity for a  $1 \rightarrow 2$  symmetric Gaussian cloning machine. Once the EPR entanglement is introduced, the two output states are expressed as

$$\hat{a}_{out2}(R=1/2) = \hat{a}_{in} - \sqrt{2}(\hat{E}_1^+ + \hat{E}_2 e^{i\theta}) / 2 \quad (S10)$$

$$\hat{a}_{out3}(R=1/2) = \hat{a}_{in} - \sqrt{2}(\hat{E}_1^+ - \hat{E}_2 e^{i\theta}) / 2 \quad (S11)$$

when  $\theta$  is set to be 0, the fidelity of output 2 is  $F_2 = 2 / (2 + e^{-2r})$  which is larger than  $2/3$  with any  $r > 0$ , and output 3 is  $F_3 = 2 / (2 + e^{2r})$  which is always smaller than  $2/3$ .

Here, we define a parameter  $V(r, \theta) = e^{-2r} \cos^2 \frac{\theta}{2} + e^{2r} \sin^2 \frac{\theta}{2}$  in which  $r$  is the squeezing parameter, according to the annihilation operator of the output state, the fidelities of two output nodes can be written as [8]:

$$F_2 = \frac{2}{2 + V(r, \theta)} \quad (S12)$$

$$F_3 = \frac{2}{2 + V(r, \theta + \pi)} \quad (S13)$$

so that the fidelities of the states at node 2 and node 3 can be controlled by the squeezing factor  $r$  and the relative phase  $\theta$  between the EPR2 and the displaced state in this case.

### Investigation of $1 \rightarrow M$ quantum state distributor

The setup can be conveniently extended to  $1 \rightarrow M$  optimal quantum state cloning by simply change  $R$  to  $(M-1)/M$ , together with  $(M-2)$  beam splitters [8]. Once  $R$  is changed to  $(M-1)/M$ , the two output states from the beam splitter BS2 are given by

$$\hat{a}_{out2} = \hat{a}_{in} - \sqrt{\frac{M-1}{M}}(\hat{E}_2 + \hat{E}_1^\dagger) \quad (S14)$$

$$\hat{a}_{out3} = \sqrt{M-1}\hat{a}_{in} - \frac{M-1}{\sqrt{M}}\hat{E}_1^\dagger + \sqrt{\frac{1}{M}}\hat{E}_2 \quad (S15)$$

so the fidelity at node 2 is calculated to be

$$F_2 = \frac{1}{1 + \frac{M-1}{M}e^{-2r}} \quad (S16)$$

A beam splitter with the reflectivity of  $(M-2)/(M-1)$  is used to split the state into two parts, the output states of this beam splitter are written as

$$\hat{a}_{out3'} = \hat{a}_{in} - \frac{M-1}{\sqrt{M(M-1)}}\hat{E}_1^\dagger + \sqrt{\frac{1}{M(M-1)}}\hat{E}_2 - \sqrt{\frac{M-2}{M-1}}\hat{V}_1 \quad (S17)$$

$$\hat{a}_{out4} = \sqrt{M-2}\hat{a}_{in} - \sqrt{\frac{(M-1)(M-2)}{M}}\hat{E}_1^\dagger + \sqrt{\frac{M-2}{M(M-1)}}\hat{E}_2 + \sqrt{\frac{1}{M-1}}\hat{V}_1 \quad (S18)$$

in which  $\hat{V}_1$  is introduced by the other side of the beam splitter. The fidelity at node 3 can be calculated by the expression of the  $\hat{a}_{out3'}$ , is given by

$$F_3 = \frac{2}{2 + \frac{M-2}{M-1} + \frac{1}{2}e^{-2r} \frac{(M-2)(M-2)}{M(M-1)} + \frac{1}{2}e^{2r} \frac{M}{M-1}} \quad (S19)$$

All the other quantum states from node 4 till node  $M+1$  have the same fidelity as the quantum state at node 3 for  $1 \rightarrow M$  optical quantum cloning.

### Fidelity of multistep quantum state distributor

In the case of  $1 \rightarrow 2$  quantum state distributor with  $R=1/2$ , the distributed states at two output nodes have the fidelity covering from 0.17 to 0.95 in virtue of the controllable distribution process. The operation scheme of the controllable quantum state distributor is easily scalable to  $2^k$  channels by a cascaded  $k$ -level distributing operation in a straightforward manner, as is shown in Fig. S4. Here, the high fidelity is essential to build cascade state distributing operations. As the distributing level is increased, the fidelity of the distributed state decreases. No matter how many levels distributing operations one tries to finish, the optimal fidelity of the distributed state at the last level should be more than the classical limit  $2/3$  that is the threshold of the quantum distributor. We define a maximum parameter  $n$  to signify how many times distributing operations are expected to be achieved sequentially.  $n$  is defined to satisfy

$\frac{2}{3} = \frac{1}{1 + ne^{-2r}/2}$ . Therefore,  $n$  can be expressed as [9]

$$n = \frac{1}{e^{-2r}} = \frac{F_{\text{exp}t}}{2 - 2F_{\text{exp}t}} \quad (S20)$$

with an experimental fidelity  $F_{\text{expt}} = \frac{1}{1 + e^{-2r}/2}$ . Here, we distribute a coherent state with a fidelity  $F=0.95 \pm 0.02$ , which is expected to achieve 9 times of distributing operations with the ultimate fidelity of surpassing the classical limit. Therefore, a quantum state can be teleported to 512 nodes connected with a distributed quantum network by manipulating EPR beams. This could be further improved by improving the fidelity of the  $1 \rightarrow 2$  quantum state distributor.

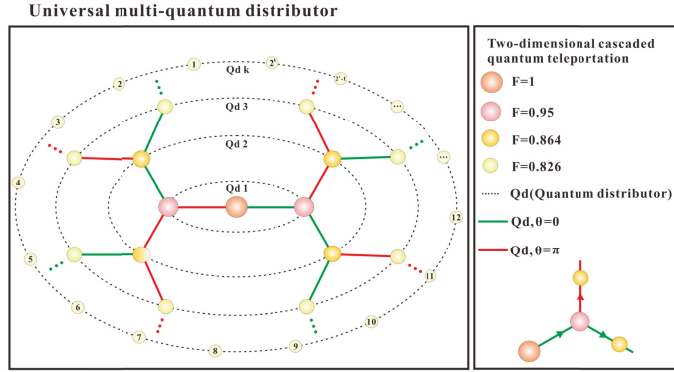


Fig. S4. Schematic diagram of a multistep quantum state distributor. Here, we show a  $2^k$ -port distributor using  $k$ -level  $1 \rightarrow 2$  distributing operations in series. Each distributing operation has two paths determined by noise variance of the EPR beam. The output state of the previous-level distributing operation is used as the input state of the next-level one.

### Information of the quantum state in the semi-quantum channel

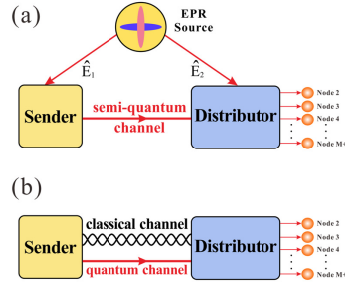


Fig. S5. Comparison of the two different distribution protocols. (a) Distribution protocol with the assistance of EPR entangled state. Due to the usage of highly entanglement, the transmitted channel can be regarded as a semi-quantum channel. (b) Distribution protocol with only linear optics. There are two channels between the sender and the distributor: most of the information of the input state is directly transmitted to the distributor through the quantum channel; the other information of the input state is transmitted through the classical channel with property gain factor.

Here, we theoretically compare the information of the quantum state in the transmitted channel of two distributor protocol, including the entanglement-assisted distribution and linear optics distribution [10]. The schematic diagram of the two protocols is shown in Fig. S5. Fig. S5(a) shows our protocol of quantum state distributor: with one half of the entangled state, the information about the input state is buried in the noise of the high entanglement. Hence the transmission channel can be regarded as a semi-quantum channel. As for the distribution protocol with only linear optics shown in Fig. S5(b), one classical channel is used to send the electronic signal with adjustable gain factor and most information of the input state is directly transmitted through the other quantum channel.

In term of  $1 \rightarrow M$  quantum state distribution, more information is destroyed at sender's station in our protocol, so less information is directly transmitted through the semi-quantum channel, leading to the less vulnerability to the potential eavesdropping. On the contrary, most of the information of the unknown state is directly transmitted through the quantum channel in the proposal with only linear optics, so it is more vulnerable to the eavesdropping.

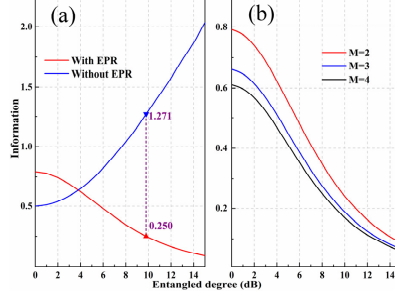


Fig. S6. Information processed through the transmitted channel. (a) The red curve represents the information processed through the semi-quantum channel as a function of the entangled degree in our protocol; the blue curve shows the information processed through the quantum channel in the protocol with only linear optics in which the fidelities at the receivers' nodes are the same as the fidelities in the protocol using EPR states with different entangled degree. (b) The information processed through the semi-quantum channel as a function of the entangled degree under different number  $M$  of receivers' nodes.

The displaced state expressed by Eq. (S6) is transmitted to the Distributor through semi-quantum channel, the information processed through this channel can be expressed by [11]

$$I = \frac{1}{2} \log_2(1 + \gamma) \quad (\text{S21})$$

in which  $\gamma$  is the signal-to-noise ratio calculated from the variances of signal and noise.

For a given  $\hat{a}_{in}$ , the displaced state is only determined by  $R$  and  $\hat{E}_1$ , so  $I$  could be determined by  $R$  and  $\hat{E}_1$  too. With the increase of entangled degree,  $I$  gets lower and lower, the information processed through the semi-quantum channel as a function of the entangled degree is shown in Fig. S6(a). In our experimental realization for  $1 \rightarrow 2$  quantum state distribution, the maximum fidelity of 0.95 is achieved, corresponding to  $I_1=0.250$ . When the same fidelity is obtained with only line optics,  $I_2=1.271$ , it is about 5.1 times than  $I_1$ . The information of the transported quantum state is submerged into the thermal noise of the EPR entanglement is the main reason that  $I_1$  becomes such low. For point-to-multipoint quantum state distribution, the information of the quantum state in the semi-quantum channel gets lower and lower with the increase of the receivers' nodes, shown in Fig. S6(b). Additionally, owing to high entangled degree, one could obtain little information of the quantum state from the semi-quantum channel with the help of EPR entanglement.

## References

1. Z. Li, W. Ma, W. Yang, Y. Wang, and Y. Zheng, "Reduction of zero baseline drift of the Pound–Drever–Hall error signal with a wedged electro-optical crystal for squeezed state generation," *Optics letters* 41, 3331-3334 (2016)
2. S. Shi, Y. Wang, W. Yang, Y. Zheng, and K. Peng, "Detection and perfect fitting of 13.2 dB squeezed vacuum states by considering green-light-induced infrared absorption," *Optics letters* 43, 5411-5414 (2018)
3. X. Sun, Y. Wang, L. Tian, Y. Zheng, and K. Peng, "Detection of 13.8 dB squeezed vacuum states by optimizing the interference efficiency and gain of balanced homodyne detection," *Chinese Optics Letters* 17, 072701 (2019)
4. H. Vahlbruch, M. Mehmet, K. Danzmann, and R. Schnabel, "Detection of 15 dB Squeezed States of Light and their Application for the Absolute Calibration of Photoelectric Quantum Efficiency," *Physical review letters* 117, 110801 (2016)
5. T. C. Zhang, K. W. Goh, C. W. Chou, P. Lodahl, and H. J. Kimble, "Quantum teleportation of light beams," *Physical Review A* 67, 033802 (2003)
6. D. T. Smithey, M. Beck, M. G. Raymer, and A. Faridani, "Measurement of the Wigner distribution and the density matrix of a light mode using optical homodyne tomography: Application to squeezed states and the vacuum," *Physical review letters* 70, 1244-1247 (1993)
7. S. L. Braunstein, C. A. Fuchs, H. J. Kimble, and P. van Loock, "Quantum versus classical domains for teleportation with continuous variables," *Physical Review A* 64, 022321 (2001)
8. J. Zhang, C. Xie, and K. Peng, "Continuous-variable quantum state transfer with partially disembodied transport," *Physical review letters* 95, 170501 (2005)

9. M. Yukawa, H. Benichi, and A. Furusawa, "High-fidelity continuous-variable quantum teleportation toward multistep quantum operations," *Physical Review A* 77, 022314 (2008)
10. Z. Zhai, J. Guo, and J. Gao, "Generalization of continuous-variable quantum cloning with linear optics," *Physical Review A* 73, 052302 (2006)
11. N. J. Cerf, M. Lévy, and G. V. Assche, "Quantum distribution of Gaussian keys using squeezed states," *Physical Review A* 63, 052311 (2001)